

Supporting Online Material for

Using Engineered Scaffold Interactions to Reshape MAP Kinase Pathway Signaling Dynamics

Caleb J. Bashor, Noah C. Helman, Shude Yan, Wendell A. Lim*

*To whom correspondence should be addressed. E-mail: lim@cmp.ucsf.edu

Published 14 March 2008, *Science* **319**, 1539 (2008)
DOI: 10.1126/science.1151153

This PDF file includes

Materials and Methods

SOM Text

Figs. S1 to S6

Tables S1 to S3

References

1. Materials and Methods

Constructs and strains

Synthetic circuits were introduced into appropriate yeast strains as two distinct plasmid-encoded components: 1) a synthetic scaffold consisting of Ste5-leucine zipper fusion and 2) recruited modulator/decoy constructs consisting of different promoters driving transcription of an modulator/decoy-zipper fusion. General architecture of constructs containing both of these components, as well as sequence details of the promoter and terminator regions used in plasmid construction are provided in **Figure S1**. All promoters, terminators, and yeast genes (*STE5*, *MSG5*, *STE50*) were cloned from a *Saccharomyces cerevisiae* genomic library (Invitrogen) by PCR.

Leucine zippers used in scaffold and modulator fusions were hetero-oligomerizing zippers designed by Vinson and colleagues that are derived from the human PAR family member VBP (*S1*). These zippers were chosen as generic recruitment modules because they were likely to be orthogonal to yeast proteins – exclusively interacting with each other. We experimentally confirmed that expression of zippers alone had no effect on the behavior of the mating pathway (**Figure S2**, panels C and D). Furthermore, there are defined mutants of the zippers that can be used to systematically tune interaction affinity over a range of 10^3 (**Figure S2A**). Details of leucine zipper sequences, identity of zipper binding partners, and binding affinities for different pairs are provided in **Figure S2**. Specific plasmid constructs used in this study are listed in **Table S1**, and the identity of the constructs used for circuit construction in each experiment are listed in **Table S2**.

Genotypes of yeast strains used in this study are listed in **Table S3**. Gene knockouts were made using standard gene disruption techniques. Unless specifically indicated, all experiments were conducted in the background strain CB011, a $\Delta far1$ strain which does not show cell cycle arrest upon α -factor treatment, and shows no shmooing behavior. Use of this strain was necessary for quantitatively reproducible FACS analysis, as *Far1*-dependent cell cycle arrest led to a wide variation in cell size and GFP expression per cell (*S2*). This strain also lacks the *Bar1* protease that degrades α -factor. For this work, this $\Delta far1\Delta bar1$ strain was arbitrarily defined to be the starting “wild-type” strain, although it has slightly different behavior from a *FAR1* strain.

STE5 synthetic scaffold constructs were derived from the parent vector HO-hisG-URA3-hisG-poly-HO (see **Figure S1** for cloning details), which was designed for genomic integration into the HO locus (*S3*). Strains harboring circuits were built from CB011 by initially integrating synthetic scaffold constructs. Modulator/decoy constructs were then introduced by genomic integration. These constructs were derived from either pRS305, which integrates into the *LEU2* locus, or pRS304 which integrates into the *TRP1* locus (*S4*). Correct genomic integration of pRS304- and pRS305-based as well as HO-locus constructs into the appropriate marker loci was verified by performing PCR on colony lysates.

Diverse response circuits

In order to realize the behaviors for circuits depicted in **Figure 4**, we made a small library of 4 to 6 configurations of a basic design in which parameters such as promoter strength

and zipper affinity were varied. From these small libraries, between 25-30% of the circuits showed the target behavior. The most interesting examples from these libraries were chosen for more careful quantitative analysis, and are depicted in **Figure 4**. A summary of which circuit configurations were constructed, and their behaviors, is summarized in **Figure S3**.

Real-time quantitative PCR

Quantitative activity of the various promoters used in this study were analyzed by RT-PCR (**Figure S4**). Total RNA was isolated from yeast by hot acid phenol extraction (S5). Extracts were treated with DNase to remove contaminating genomic DNA, and template cDNA was synthesized from 1-3 µg total RNA using T18 as a primer. To further ensure that only cDNA and not genomic DNA was amplified during the PCR, controls were run to which no reverse transcriptase was added. Real time, quantitative PCR was done using a DNA engine Opticon machine (BioRad) with SYBR green as the fluorescent probe. Relative mRNA expression level of each measured gene in a given sample was determined by normalization to the transcript level of the gene *TDH1*.

Flow cytometry

Analysis of pathway-dependent GFP expression by flow cytometry was performed largely as described (S6) with the following specific modifications: For all FACS-GFP experiments, triplicate cultures were grown to early log phase ($OD_{600}=0.05-0.1$) in complete synthetic dropout media. For time course experiments, triplicate cultures were treated with 2 µM α-factor (Zymo Research) to initiate the pathway. For dose-response experiments, three separate cultures were treated with each of the indicated α-factor concentrations. For time course experiments, aliquots of cultures were removed at 15 min intervals. For dose-response experiments, cultures were sampled once at indicated times. For both types of experiments, sample aliquots were treated with cycloheximide (5µg/mL), and dispensed into 96-well culture plates. Following incubation at room temperature for 1 hr in the dark to allow for GFP fluorophore maturation, plates containing treated cultures were analyzed with a BD LSR-II flow cytometer (BD Biosciences) using a high-throughput sampling module. 5,000 cells were counted for each reading, and GFP fluorescence was measured by exciting at 488 nm with a 100 mW Coherent Sapphire laser.

Analysis of FACS-GFP fluorescence data for α-factor-treated cell populations has been described previously (S6). For the present study, mean fluorescence intensity data in time course experiments were converted to the transcriptional rate data plots seen in **Figures 2, 3, and 4**. This conversion was carried out to more accurately reflect the temporal variation in pathway output – absolute GFP expression is a poor direct readout of this, since the apparent lifetime of the GFP used here is >100 minutes, and thus it continuously accumulates over the course of the experiment. Transcriptional activity was calculated according to the process outlined in **Figure S5**, by taking into account GFP synthesis and degradation/dilution. Data points in figures containing time course data represent mean transcriptional activity values for triplicate experiments ± std. dev. Solid line fits in these figures represent solutions to a quantitative dynamic model consisting of coupled differential equations (see “Quantitative Modeling” section).

Data points in figures containing dose-response data represent mean fluorescence intensity values for triplicate experiments \pm std. dev. Triplicate data from dose-response profiles were fitted using ProFit software (Quantum Soft) to a Hill equation: $F(a) = (F_{\min} + (F_{\max} - F_{\min})) * (a^{(n_H)} / (C_m^{(n_H)} + a^{(n_H)}))$, where F = mean fluorescence, a = concentration of α -factor, F_{\min} = mean basal fluorescence (no α -factor), F_{\max} = mean fluorescence with maximal pathway output (saturating α -factor), C_m = α -factor concentration at which fluorescence is half-maximal, and n_H = Hill coefficient. Error for Hill coefficients are std. dev. values determined by the Profit curve fitting algorithm and reflect errors amongst experimental replicates.

Analysis of Fus3 phosphorylation by western blotting

Yeast cells in mid-log phase ($OD_{600}=0.5$) were treated with saturating α -factor (2 μ M) and 5 mL of culture was harvested at indicated time points. Samples were prepared from harvested cells for western blot experiments by lysis in SDS-PAGE buffer (350 μ L) and ~20 μ L of sample were used for immunoblot detection. Phosphorylated Fus3 was detected using an anti-phospho p44/42 antibody (Cell Signaling Technology) as primary followed by Goat anti-Rabbit IR@800 secondary (Odyssey). Blots were visualized using a LICOR Odyssey infrared imager. For hexokinase loading controls (see **Figure S6**), blots were stripped and reprobed with a yeast hexokinase antibody (US Biological, H2305-01) followed by LICOR detection using the same Goat anti-Rabbit IR@800 secondary.

2. SOM Text—Quantitative Modeling

To assess whether the behaviors of the synthetic feedback circuits could be explained by the simple model of dynamically-regulated recruitment to the scaffold, we simulated pathway behavior using a system of three coupled ordinary differential equations (see below), tracking the activation states of the scaffold complex and a transcription factor and the population of the feedback modulator. Fits to the experimentally observed transcriptional activity (**Figures 2-4**) are derived from this model.

In this highly simplified model, the scaffold complex was considered as a lumped element (i.e. black box) with a fixed total population comprised of two states: active and inactive. The total population of the transcription factor was also assumed constant, and similarly composed of active and inactive versions. Scaffolds were activated by pheromone input with Michaelis-Menten kinetics. Inactive transcription factors were activated by active scaffolds. The population of active transcription factor was the computational readout, which we compared against the experimentally measured transcriptional activity (see **Figure S5**).

To model feedback circuits, synthesis of modulator proteins from mating-responsive promoters was modeled as a function of active transcription factor using a Hill equation ($n_H = 2$; this closely matches experimentally observed expression from the mating responsive promoter *pFIG1* – see **Figure S4**). The binding of the synthesized feedback modulator to the scaffold complex was explicitly calculated using a dissociation constant corresponding to the affinity of the leucine zippers. Negative (positive) feedback modulator bound to the scaffold reduced (increased) the concentration of active scaffolds

at a significantly higher rate than unbound feedback elements. For circuits that consist of multiple binding partners (e.g. feedback element that can bind to either the scaffold or a decoy element), the populations of the possible binding complexes were calculated explicitly by computationally solving a cubic equation, assuming that the populations come to binding equilibrium on a time scale short with respect to the other time scales in the equations. Furthermore, the simulation began 100 min before the α -factor stimulus was added in order to allow the system to reach an uninduced equilibrium. Most parameters were kept constant amongst all circuits: activation rates, dissociation constants, decay constants, catalytic constants, total populations of scaffold and transcription factors, etc. Parameters that were allowed to vary somewhat include background basal scaffold activity and promoter strengths (we have observed that expression from a single promoter varied over a range of ~5-10 fold on average from clone to clone on a single genomic integration transformation).

The equations below were used to represent the synthetic feedback circuits. The first set of equations, describing the dynamics of transcription factor activation and feedback element transcription as well as conservation rules, are common to all simulations. The system of ordinary differential equations was solved computationally for each circuit using built-in functions in MATLAB (Mathworks, Natick, MA). Code available upon request.

Equations used for simulating circuits:

Common to all circuits:

$$\frac{dTF_{active}}{dt} = (k_{TF}Scaffold_{active})TF_{inactive} - \gamma_{TF}TF_{active}$$

$$\frac{dFB}{dt} = k_{FB} \frac{TF_{active}^{n_H}}{k_{d-TF}^{n_H} + TF_{active}^{n_H}} + k_{FBbasal} - \gamma_{FB}FB$$

$$1 = f_{bound} + f_{unbound}$$

$$Scaffold_{TOTAL} = Scaffold_{active} + Scaffold_{inactive}$$

$$TF_{TOTAL} = TF_{active} + TF_{inactive}$$

Negative feedback:

$$\begin{aligned} \frac{dScaffold_{active}}{dt} = & \frac{S_\alpha}{k_\alpha + S_\alpha} Scaffold_{inactive} f_{unbound} - \gamma_{scaffold} Scaffold_{active} \\ & - (f_{bound_neg} k_{cat_neg}) Scaffold_{active} \\ & - (f_{unbound} k_{cat_neg} k_{cat-off-scaffold_ratio}) FB_{unbound} Scaffold_{active} \end{aligned}$$

Positive feedback:

$$\begin{aligned} \frac{dScaffold_{active}}{dt} = & \frac{S_\alpha}{k_\alpha + S_\alpha} Scaffold_{inactive} f_{unbound} - \gamma_{scaffold} Scaffold_{active} \\ & + (f_{bound_pos} k_{cat_pos}) Scaffold_{inactive} \\ & + (f_{unbound} k_{cat_pos} k_{cat-off-scaffold_ratio}) FB_{unbound} Scaffold_{inactive} \end{aligned}$$

Accelerator:

$$\begin{aligned} \frac{dScaffold_{active}}{dt} = & \frac{S_\alpha}{k_\alpha + S_\alpha} Scaffold_{inactive} f_{unbound} - \gamma_{scaffold} Scaffold_{active} \\ & + (f_{bound_pos} k_{cat_pos}) Scaffold_{inactive} \\ & + f_{unbound} k_{cat_pos} k_{cat-off-scaffold_ratio} Ste50_{unbound} Scaffold_{inactive} \\ & - (f_{bound_neg} k_{cat_neg}) Scaffold_{active} \\ & - (f_{unbound} k_{cat_neg} k_{cat-off-scaffold_ratio}) FB_{unbound} Scaffold_{active} \end{aligned}$$

Delay:

$$\begin{aligned} \frac{dScaffold_{active}}{dt} = & \frac{S_\alpha}{k_\alpha + S_\alpha} Scaffold_{inactive} f_{unbound} - \gamma_{scaffold} Scaffold_{active} \\ & - (f_{bound_neg} k_{cat_neg}) Scaffold_{active} \\ & - (f_{unbound} k_{cat_neg} k_{cat-off-scaffold_ratio}) FB_{unbound} Scaffold_{active} \end{aligned}$$

Variables (concentrations):

$Scaffold_{active}$ = lumped element variable that represents the activated MAPK pathway (note: $Scaffold_{TOTAL}$ = fixed value)

TF_{active} = activated transcription factor

FB = feedback modulator concentrator

Parameters:

Kinetic rate constants:

k_{TF} = rate constant for activation of inactive transcription factor via active Scaffold

k_{FB} = rate constant for creation of feedback modulator via active transcription factor

$k_{FBbasal}$ = basal rate of creation of feedback modulator (in absence of pheromone)

γ_{TF} = endogenous decay rate of active TF_{active} to inactive $TF_{inactive}$

γ_{FB} = endogenous degradation rate of FB

$\gamma_{scaffold}$ = endogenous decay rate of active scaffold complex to inactive scaffold complex

Binding constants:

k_α = binding constant of α -factor

k_{d-TF} = dissociation constant of TF from promoter of FB

Catalytic constants:

k_{cat} = catalytic rate of feedback modulator (e.g. rate constant for phosphatase converting active scaffolds to inactive scaffolds)

$k_{cat-off-scaffold-ratio}$ = ratio corresponding to reduced effectiveness of unbound effectors to catalyze reactions on the scaffold.

Other constants:

S_α = concentration of α -factor (strength of α -factor signal)

f_{bound_neg} = fraction of scaffolds bound by the negative feedback modulator (between 0-1)

f_{bound_pos} = fraction of scaffolds bound by the positive feedback modulator (between 0-1)

$f_{unbound}$ = fraction of scaffolds not bound by any feedback modulator (between 0-1)

n_H = Hill coefficient for transcription of feedback gene

$Ste50_{unbound}$ = Total Ste50 (fixed value) minus Ste50 bound in complex with Scaffold.

In order to calculate the concentration of complexes with competing molecular species, the assumption that the binding reactions come to equilibrium on a fast time scale compared to other system dynamics leads to a cubic equation that can be solved

numerically. Specifically, consider three molecular species A, B, and C which can form complexes AB and BC (but not AC) – namely, A and C compete for binding to B. If k_1 is the dissociation constant for A binding to B and k_2 is the dissociation constant for C binding to B, then the concentration of the complex AB is the solution of the following equation which is between zero and the smaller of A_T and B_T , where:

$$a \cdot [AB]^3 + b \cdot [AB]^2 + c \cdot [AB] + d = 0$$

$$k = k_1 / k_2$$

$$a = k - 1$$

$$b = 2A_T + B_T + k_1 + k \cdot (C_T - B_T - A_T - k_1)$$

$$c = -A_T \cdot (A_T + 2B_T + k_1 + k(C_T - B_T))$$

$$d = A_T^2 B_T$$

Parameters:

Global (common to all simulations):

k_α	20
k_{TF}	0.004
γ_{TF}	0.018
$\gamma_{scaffold}$	0.2
k_d weak zipper	150
k_d medium zipper	15
k_d strong zipper	5
k_{d-TF}	6
TF_{TOTAL}	50
$Scaffold_{TOTAL}$	50
k_{cat} negative feedback	0.5
k_{cat} positive feedback	1
k_{FB} strong basal ratio	0.028
k_{FB} weak basal ratio	0.059
$k_{cat_off_scaffold_ratio}$	0.006
n_{Hill}	2

Circuit-specific parameters:**Parameters for Figure 2 (simple negative and positive feedback):**

circuit	negative feedback	positive feedback
feedback promoter	strong	strong
zipper	medium	medium
S_α basal	0.003	0.01
k_{TF}	2.1	0.75
γ_{FB}	0.0025	0.001

Parameters for Figure 3 (variations of negative feedback):

feedback promoter	strong	strong	strong	weak	weak	weak
zipper	strong	medium	weak	strong	medium	weak
S_α basal	0.018	0.003	0.002	0.018	0.001	0.015
k_{TF}	1.5	2.1	2.1	1	2.1	0.5
γ_{FB}	0.0025	0.0025	0.0025	0.0025	0.0025	0.0025

Parameters for Figure 4 (circuits with binding competition):

circuit	decoy	decoy	decoy	accelerator	delay
feedback promoter	strong	weak	none	strong	strong
Zipper	decoy-strong; Msg5-medium	decoy-strong; Msg5-medium	Msg5-medium	Ste50-medium; Msg5-strong	decoy-medium; Msg5-strong
S_α basal	0.0015	0.02	0.005	0	0.05
k_{TF}	2.85	2.25	2.55	4.35	12
Decoy _{TOTAL}	300	150	0	0	
Ste50 _{constitutive_TOT_AL}				35	
Msg5 _{constitutive_TOT_AL}					280
γ_{FB}	0.0025	0.0025	0.0025	0.0025	0.0005

Figure S1

Synthetic Scaffolds



Recruited Effectors



Promoter	Effector/Decoy	Zipper	ADH1 Terminator
<i>ADH1</i>	<i>MSG5</i>		
<i>CYC1</i>	<i>STE50</i>		
<i>STE5</i>	<i>GST</i>		
<i>FIG1</i>			
<i>PRM2</i>			

Promoter regions used (bases upstream of start)	
<i>ADH1</i>	1.5 kb
<i>CYC1</i>	250 bp
<i>STE5</i>	600 bp
<i>FIG1</i>	600 bp
<i>PRM2</i>	600 bp

Terminator regions used (bases downstream of stop)	
<i>ADH1</i>	200 bp
<i>STE5</i>	500 bp

Figure S1. Modular construction of circuit components. All vectors used in the construction of synthetic scaffold and recruited effector elements were constructed according to the architecture depicted here (See **Table S1** for complete list of constructs used in this study). Sequences for modulator/decoy elements were cloned as XhoI/BamHI fragments and contained the entire open reading frame for each gene except for the start ATG and stop codons. For recruited modulator constructs, indicated promoter regions were cloned as ApaI and XhoI fragments included the start codon from the open reading frame of corresponding genes. For synthetic scaffold constructs, 500 bp of *pSTE5* promoter was cloned with the *STE5* open reading frame as a single BglII and BamHI or ApaI and BamHI fragment. Zipper sequences were cloned into both scaffold and modulator constructs as BamHI and NotI fragments (see **Figure S2** for sequence details) and included a TAG stop codon immediately following their coding sequences. The indicated terminator regions were cloned as NotI and SacI fragments. Synthetic scaffold cassettes were cloned into the HO-hisG-URA3-hisG-poly-HO multiple cloning site, modulator cassettes were cloned into pRS304 and pRS305 vectors (see **Table S1** for list of constructs and their parent vectors).

Figure S2

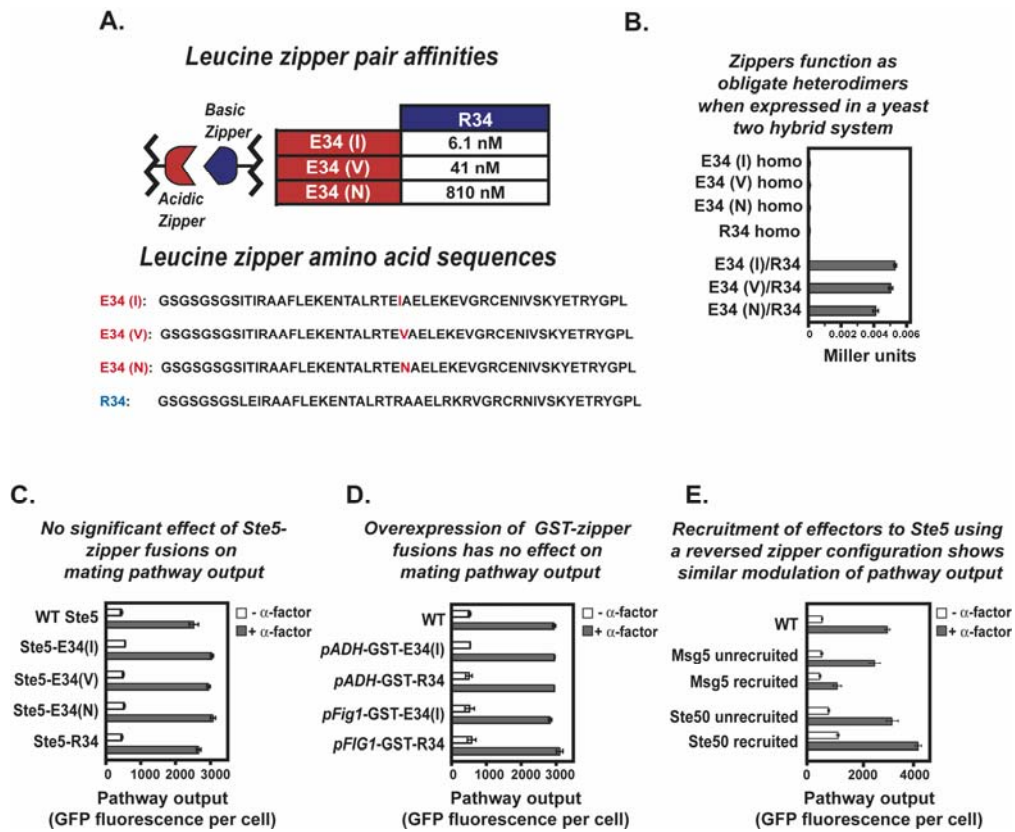
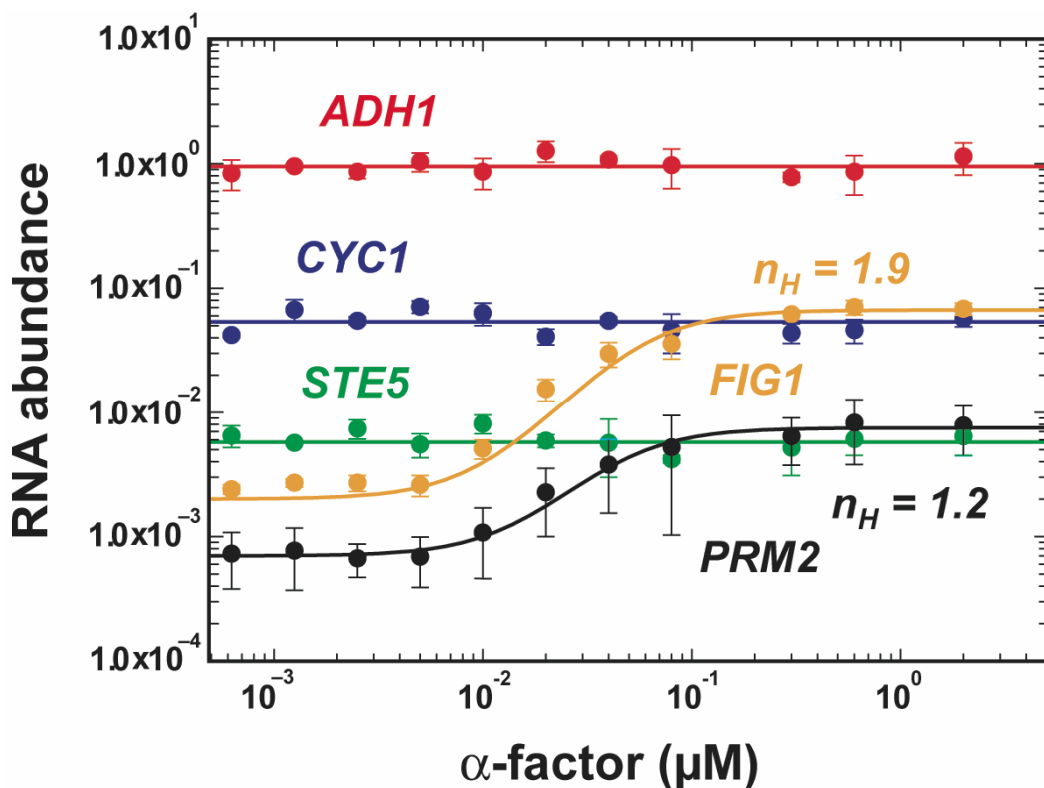


Figure S2. Leucine zippers used in circuit construction. (A) Specific heterooligomeric zipper interactions: zipper sequences and corresponding affinities. These leucine zippers were initially characterized by Vinson and colleagues (*SJ*). (B) Yeast two-hybrid experiments demonstrate that zippers behave as obligate hetero-dimers *in vivo*. For heterodimerizing pairs, acidic zippers were used as bait and basic zippers were used as prey. Error bars represent standard deviation for three experiments. (C) Fusing leucine zippers to Ste5 does not significantly affect pathway output (see **Figure S1** for construct details). The strain CB011 (see **Table S3**) was transformed with plasmids coding for Ste5-zipper fusions (CB551, CB552, CB553, and CB554) and assessed for pathway activity in the absence of effectors by GFP FACS after treatment with 2 μM α-factor for two hours. Error bars represent standard deviation for three experiments. (D) Overexpression of leucine zippers has no significant effect on mating pathway output. The strain CB009 (see **Table S3**) was transformed with plasmids coding for GST-zipper fusions (CB531, CB532, CB524, CB525) and assessed for pathway activity by GFP FACS after two hours of 2 μM α-factor treatment. Error bars represent standard deviation for three experiments. (E) Leucine zipper configuration with acidic zipper fused to Ste5 and the basic zipper fused to effectors show qualitatively similar results to the experiment in **Figure 1B** (where basic zipper is fused to Ste5 and acidic zipper is fused to Msg5). The experiment was conducted in the same manner as described for **Figure 1B**.

Figure S3

<i>Design</i>	<i>recruitment interactions (zippers - FIXED)</i>	<i>promoters (VARIABLE)</i>	<i>Behavior Class</i>														
PULSE		scaffold: E34-V (med) decoy: E34-I (strong) neg.mod.: R34	<table border="1"> <thead> <tr> <th><i>Decoy (constitutive)</i></th> <th><i>Neg. Modulator (induced)</i></th> </tr> </thead> <tbody> <tr> <td>low (<i>pST5</i>)</td> <td>low (<i>pPRM2</i>)</td> </tr> <tr> <td>med (<i>pCYC1</i>)</td> <td>low (<i>pPRM2</i>)</td> </tr> <tr> <td>high (<i>pADH1</i>)</td> <td>low (<i>pPRM2</i>)</td> </tr> <tr> <td>low (<i>pST5</i>)</td> <td>high (<i>pFIG1</i>)</td> </tr> <tr> <td>med (<i>pCYC1</i>)</td> <td>high (<i>pFIG1</i>)</td> </tr> <tr> <td>high (<i>pADH1</i>)</td> <td>high (<i>pFIG1</i>)</td> </tr> </tbody> </table> <p>adaptation adaptation adaptation pulse (Fig. 4A) pulse pulse (Fig. 4A)</p>	<i>Decoy (constitutive)</i>	<i>Neg. Modulator (induced)</i>	low (<i>pST5</i>)	low (<i>pPRM2</i>)	med (<i>pCYC1</i>)	low (<i>pPRM2</i>)	high (<i>pADH1</i>)	low (<i>pPRM2</i>)	low (<i>pST5</i>)	high (<i>pFIG1</i>)	med (<i>pCYC1</i>)	high (<i>pFIG1</i>)	high (<i>pADH1</i>)	high (<i>pFIG1</i>)
<i>Decoy (constitutive)</i>	<i>Neg. Modulator (induced)</i>																
low (<i>pST5</i>)	low (<i>pPRM2</i>)																
med (<i>pCYC1</i>)	low (<i>pPRM2</i>)																
high (<i>pADH1</i>)	low (<i>pPRM2</i>)																
low (<i>pST5</i>)	high (<i>pFIG1</i>)																
med (<i>pCYC1</i>)	high (<i>pFIG1</i>)																
high (<i>pADH1</i>)	high (<i>pFIG1</i>)																
ACCELERATOR		scaffold: E34-V (med) pos.mod.: R34 neg.mod.: R34	<table border="1"> <thead> <tr> <th><i>Pos. Modulator (constitutive)</i></th> <th><i>Neg. Modulator (induced)</i></th> </tr> </thead> <tbody> <tr> <td>low (<i>pST5</i>)</td> <td>low (<i>pPRM2</i>)</td> </tr> <tr> <td>med (<i>pCYC1</i>)</td> <td>low (<i>pPRM2</i>)</td> </tr> <tr> <td>low (<i>pST5</i>)</td> <td>high (<i>pFIG1</i>)</td> </tr> <tr> <td>med (<i>pCYC1</i>)</td> <td>high (<i>pFIG1</i>)</td> </tr> </tbody> </table> <p>adaptation adaptation accelerator (Fig. 4B) high activation</p>	<i>Pos. Modulator (constitutive)</i>	<i>Neg. Modulator (induced)</i>	low (<i>pST5</i>)	low (<i>pPRM2</i>)	med (<i>pCYC1</i>)	low (<i>pPRM2</i>)	low (<i>pST5</i>)	high (<i>pFIG1</i>)	med (<i>pCYC1</i>)	high (<i>pFIG1</i>)				
<i>Pos. Modulator (constitutive)</i>	<i>Neg. Modulator (induced)</i>																
low (<i>pST5</i>)	low (<i>pPRM2</i>)																
med (<i>pCYC1</i>)	low (<i>pPRM2</i>)																
low (<i>pST5</i>)	high (<i>pFIG1</i>)																
med (<i>pCYC1</i>)	high (<i>pFIG1</i>)																
DELAY		scaffold: E34-V (med) neg.mod.: E34-V (med) decoy: E34-I (strong)	<table border="1"> <thead> <tr> <th><i>Neg. Modulator (constitutive)</i></th> <th><i>Decoy (induced)</i></th> </tr> </thead> <tbody> <tr> <td>low (<i>pST5</i>)</td> <td>low (<i>pPRM2</i>)</td> </tr> <tr> <td>med (<i>pCYC1</i>)</td> <td>low (<i>pPRM2</i>)</td> </tr> <tr> <td>low (<i>pST5</i>)</td> <td>high (<i>pFIG1</i>)</td> </tr> <tr> <td>med (<i>pCYC1</i>)</td> <td>high (<i>pFIG1</i>)</td> </tr> </tbody> </table> <p>delay (Fig. 4C) weak activation weak activation weak activation</p>	<i>Neg. Modulator (constitutive)</i>	<i>Decoy (induced)</i>	low (<i>pST5</i>)	low (<i>pPRM2</i>)	med (<i>pCYC1</i>)	low (<i>pPRM2</i>)	low (<i>pST5</i>)	high (<i>pFIG1</i>)	med (<i>pCYC1</i>)	high (<i>pFIG1</i>)				
<i>Neg. Modulator (constitutive)</i>	<i>Decoy (induced)</i>																
low (<i>pST5</i>)	low (<i>pPRM2</i>)																
med (<i>pCYC1</i>)	low (<i>pPRM2</i>)																
low (<i>pST5</i>)	high (<i>pFIG1</i>)																
med (<i>pCYC1</i>)	high (<i>pFIG1</i>)																
SWITCH		scaffold: R34 pos. mod.: E34-V (med) neg. mod.: E34-I (strong)	<table border="1"> <thead> <tr> <th><i>Neg. Modulator (constitutive)</i></th> <th><i>Pos. Modulator (induced)</i></th> </tr> </thead> <tbody> <tr> <td>low (<i>pST5</i>)</td> <td>low (<i>pRM2</i>)</td> </tr> <tr> <td>med (<i>pCYC1</i>)</td> <td>low (<i>pRM2</i>)</td> </tr> <tr> <td>low (<i>pST5</i>)</td> <td>high (<i>pFIG1</i>)</td> </tr> <tr> <td>med (<i>pCYC1</i>)</td> <td>high (<i>pFIG1</i>)</td> </tr> </tbody> </table> <p>weak activation weak activation switch-like (Fig. 4D) weak activation</p>	<i>Neg. Modulator (constitutive)</i>	<i>Pos. Modulator (induced)</i>	low (<i>pST5</i>)	low (<i>pRM2</i>)	med (<i>pCYC1</i>)	low (<i>pRM2</i>)	low (<i>pST5</i>)	high (<i>pFIG1</i>)	med (<i>pCYC1</i>)	high (<i>pFIG1</i>)				
<i>Neg. Modulator (constitutive)</i>	<i>Pos. Modulator (induced)</i>																
low (<i>pST5</i>)	low (<i>pRM2</i>)																
med (<i>pCYC1</i>)	low (<i>pRM2</i>)																
low (<i>pST5</i>)	high (<i>pFIG1</i>)																
med (<i>pCYC1</i>)	high (<i>pFIG1</i>)																

Figure S3. Summary of circuit configurations tested during the construction of circuits in Figure 4. For each of the four circuit architectures depicted in **Figure 4**, multiple combinations of promoters and zippers were tested in order to determine which configurations yielded the target behaviors (pulse, acceleration, and delay time profiles, as well as switch-like dose response). For each circuit architecture, those configurations which demonstrated the richest behavior were selected for display in **Figure 4**. All constructs listed here were generated using the cloning strategy summarized in **Figure S1**. Plots represent idealizations of characteristic temporal and dose-response behaviors.

Figure S4**Figure S4. RT-PCR characterization of promoters used in circuit construction.**

In order to identify promoters that were appropriate for circuit design, we measured mRNA transcript levels from housekeeping genes and mating pathway inducible genes by RT-PCR (see materials and methods for experimental details). Promoters identified for constitutive expression of circuit components, *pADH1*, *pCYC1*, and *pSTE5*, show no expression dependence on α -factor, while promoters used for feedback of circuit components, *pFIG1* and *pPRM2*, showed dose-dependent transcriptional enhancement. Error bars represent standard deviation for three separate experiments. Dose-response profiles were fitted with a Hill equation: $R(a) = (R_{\min} + (R_{\max} - R_{\min})) * (a^{(n_H)}) / (C_m^{(n_H)} + a^{(n_H)})$, where R = mean RNA abundance, a = concentration of α -factor, R_{\min} = mean basal RNA abundance (no α -factor), R_{\max} = mean fluorescence with maximal pathway output (saturating α -factor), C_m = α -factor concentration at which RNA abundance is half-maximal, and n_H = Hill coefficient.

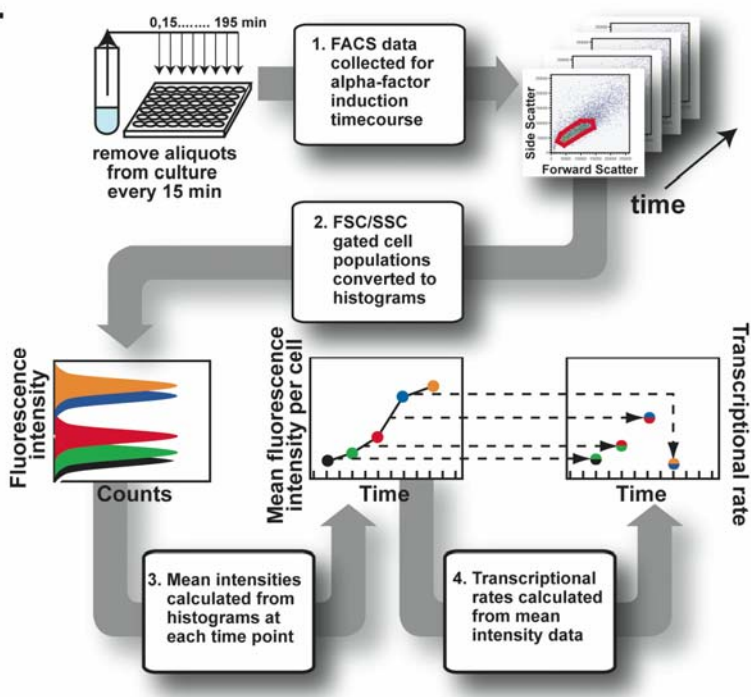
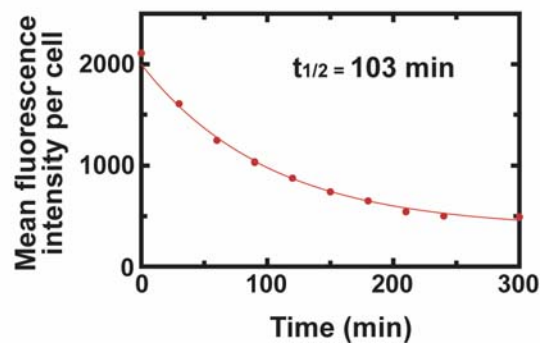
Figure S5**A.****B.**

Figure S5. Processing of data from flow cytometry experiments. (A). Determination of transcriptional rates from GFP-FACS data. All data were analyzed for fluorescence values using the program Flowjo (Treestar). In order to determine mean fluorescence intensities at times after α -factor treatment, cell populations were gated in FSC vs. SSC plots to ensure that cells of similar size and shape were compared amongst different samples and different time points. Mean fluorescence intensity data were then determined for gated populations (see S6 for a more detail description of mean fluorescence intensity determination).

For time-dependent experiments, fluorescence intensity data were measured at 15 minute intervals. These data were converted into transcriptional rates to more accurately reflect

temporal variation in pathway output – GFP expression is a poor readout of this, since the apparent lifetime of the GFP used here is >100 minutes, and thus it continuously accumulates over the course of the experiment. Data were converted using the following equation:

$$\text{Rate}_t = ((I_{t+7.5\text{min}} - I_{t-7.5\text{min}})/15 \text{ min}) + (k_{\text{decay}}(I_{t+7.5\text{min}} + I_{t-7.5\text{min}})/2)$$

Where I is mean fluorescence intensity per cell at a given time point, and k_{decay} is the decay rate of GFP in the absence of α -factor (a combination of GFP degradation and dilution by cell growth). We are essentially taking the time derivative of the observed intensities, after subtracting the intrinsic GFP decay rate. Transcriptional rates are therefore calculated for time points (t) between each pair of intensity measurements ($t+7.5$ min and $t-7.5$ min).

(B) Experimental measurement of k_{decay} (decay rate of GFP signal in cells) using an α -factor washout experiment. CB009 cells grown in liquid cultures to early log phase ($\text{OD}_{600}=0.05$) were treated with α -factor for two hours, and then washed by centrifugation and resuspension in fresh media to remove α -factor. Following one hour, the data were fitted with the following equation:

$$I_{\text{fluor}} = I_0 * e^{-k_{\text{decay}} * t}$$

Where I_{fluor} = fluorescence intensity, I_0 = initial intensity ($t=0$), t = time.

Figure S6

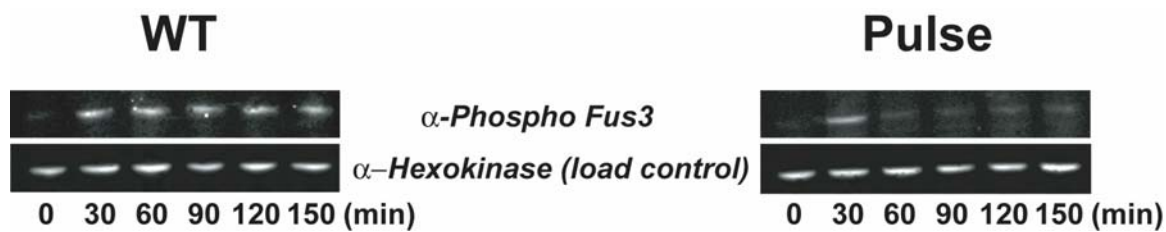


Figure S6. Loading controls for western blotting experiment. In order to control for sample loading, blots from the western blotting experiment shown in **Figure 4A** were stripped and reprobed with an anti-hexokinase antibody and analyzed using fluorescence detection (see Supplemental Methods).

Table S1. Plamids used in this study

Plasmid	Parent vector	promoter	gene	Leucine zipper
CB500	pRS305	<i>pCYC1</i>	<i>MSG5</i>	R34
CB501	pRS305	<i>pCYC1</i>	<i>MSG5</i>	E34(I)
CB502	pRS305	<i>pCYC1</i>	<i>MSG5</i>	E34(V)
CB503	pRS305	<i>pCYC1</i>	<i>MSG5</i>	E34(N)
CB504	pRS305	<i>pSTE5</i>	<i>MSG5</i>	R34
CB505	pRS305	<i>pSTE5</i>	<i>MSG5</i>	E34(I)
CB506	pRS305	<i>pSTE5</i>	<i>MSG5</i>	E34(V)
CB507	pRS305	<i>pSTE5</i>	<i>MSG5</i>	E34(N)
CB508	pRS305	<i>pFIG1</i>	<i>MSG5</i>	R34
CB509	pRS305	<i>pFIG1</i>	<i>MSG5</i>	E34(I)
CB510	pRS305	<i>pFIG1</i>	<i>MSG5</i>	E34(V)
CB511	pRS305	<i>pFIG1</i>	<i>MSG5</i>	E34(N)
CB512	pRS305	<i>pPRM2</i>	<i>MSG5</i>	R34
CB513	pRS305	<i>pPRM2</i>	<i>MSG5</i>	E34(I)
CB514	pRS305	<i>pPRM2</i>	<i>MSG5</i>	E34(V)
CB515	pRS305	<i>pPRM2</i>	<i>MSG5</i>	E34(N)
CB517	pRS304	<i>pCYC1</i>	<i>GST</i>	E34(I)
CB521	pRS304	<i>pSTE5</i>	<i>GST</i>	E34(I)
CB524	PRS304	<i>pFIG1</i>	<i>GST</i>	R34
CB525	pRS304	<i>pFIG1</i>	<i>GST</i>	E34(I)
CB531	PRS304	<i>pADH1</i>	<i>GST</i>	R34
CB532	pRS304	<i>pADH1</i>	<i>GST</i>	E34(I)
CB536	pRS304	<i>pCYC1</i>	<i>STE50</i>	R34
CB535	pRS304	<i>pCYC1</i>	<i>STE50</i>	E34(I)
CB538	pRS304	<i>pSTE5</i>	<i>STE50</i>	R34
CB541	pRS304	<i>pFIG1</i>	<i>STE50</i>	R34
CB542	pRS304	<i>pFIG1</i>	<i>STE50</i>	E33(I)
CB551	M4366	<i>pSTE5</i>	<i>STE5</i>	R34
CB552	M4366	<i>pSTE5</i>	<i>STE5</i>	E34(I)
CB553	M4366	<i>pSTE5</i>	<i>STE5</i>	E34(V)
CB554	M4366	<i>pSTE5</i>	<i>STE5</i>	E34(N)

Table S2. Plasmids used in specific experiments

Figure/Panel	Constructs used	
	Scaffold	Effector
Figure 1B	CB551	Msg5: CB500, CB501, Ste50: CB535, CB536
Figure 2A	CB551	neg. feedback: CB502 pos. feedback: CB542
Figure 3B	CB551	Strong zipper: CB513 Medium zipper: CB514 Weak zipper: CB515
Figure 3C	CB551	strong promoter: CB511 weak promoter: CB515
Figure 4A	CB553	no decoy: CB508 low decoy: CB508, CB521 high decoy: CB508, CB532
Figure 4B	CB553	neg feedback only: CB508 accelerator circuit: CB538
Figure 4C	CB553	Neg effector only: CB504 Delay circuit: CB525
Figure 4D	CB553	Switch: CB506, CB542

Table S3. Strains used in this study

Strain	Description
CB011	<i>W303 MATa, ste5::KanR, bar1::NatR, far1Δ, mfa2::pFUS1-GFP, his3, trp1, leu2, ura3</i>
CB009	<i>W303 MATa, bar1::NatR, far1Δ, mfa2::pFUS1-GFP, his3, trp1, leu2, ura3</i>

Supplemental References

1. A. Acharya, S. B. Ruvinov, J. Gal, C. Vinson, *Biochemistry* **41**, 14122-31 (2002).
2. A. Coman-Lerner, A. Gordon, E. Sera, T. Chin, O. Resnekov, D. Endy, C. G. Pesce, R. Brent, *Nature* **437**, 631-2 (2005).
3. W. P. Voth, J. D. Richards, J. M. Shaw, D. J. Stillman, *Nucleic Acids Research* **29**, 59 (2001).
4. R. S. Sikorsky, Hieter P., *Genetics* **122**, 19 (1989).
5. J. L. Derisi, V. R. Iyer, P. O. Brown, *Science* **278**, 689 (1997).
6. R. P Bhattacharyya, A. Remenyi, M.C. Good, C.J. Bashor, A.M. Falick, W.A. Lim, *Science* **311**, 822 (2006).